ARTICLE

Experimental and Theoretical Study of Hydrogen Atom Abstraction from Ethylene by Stoichiometric Zirconium Oxide Clusters[†]

Xiao-nan Wu[a,b], Yan-xia Zhao[a,b], Sheng-gui He[a*], Xun-lei Ding[a*]

a. Beijing National Laboratory for Molecular Sciences, State Key Laboratory for Structural Chemistry of Unstable and Stable Species, Institute of Chemistry, Chinese Academy of Sciences, Beijing 100190, China

b. Graduate University of the Chinese Academy of Sciences, Beijing 100049, China

(Dated: Received on August 27, 2009; Accepted on October 20, 2009)

The reactions of cationic zirconium oxide clusters ($Zr_xO_y^+$) with ethylene (C_2H_4) were investigated by using a time-of-flight mass spectrometer coupled with a laser ablation/supersonic expansion cluster source. Some hydrogen containing products $(ZrO_2)_xH^+$(x=1−4) were observed after the reaction. The density functional theory calculations indicate that apart from the common oxygen transfer reaction channel, the hydrogen abstraction channel can also occur in $(ZrO_2)_x^+ + C_2H_4$, which supports that the observed $(ZrO_2)_xH^+$ may be due to $(ZrO_2)_x^+ + C_2H_4 \rightarrow (ZrO_2)_xH^+ + C_2H_3$. The rate constants of different reaction channels were also calculated by Rice-Ramsberger-Kassel-Marcus theory.

Key words: Time-of-flight mass spectrometer, Zirconium oxide clusters, Fast flow reactor, Density functional theory, Rice-Ramsberger-Kassel-Marcus theory

I. INTRODUCTION

The chemical reactivity of transition metal oxide clusters has been widely studied with experimentally and theoretically [1,2]. The studies revealed the mechanisms of some important reactions and gave guide for new catalysts design. What is more, based on the knowledge of the reactivity and other properties of small clusters, it is possible to use the selected clusters as building blocks to assemble desirable catalyst with remarkable activity and selectivity for specific reactions [3].

Due to its high stability over a wide temperature range and its resistance to poisoning, bulk-phase zirconia (ZrO_2) is employed as both a catalyst and catalyst-support material for many reactions, such as the oxidation of CH_4 [4] and CO [5], and the epoxidation of propylene [6]. It has been revealed that cationic clusters of a particular size and stoichiometry often exhibit more greatly enhanced reactivity than bulk material [7]. Thus, the study on the reactivity of cationic zirconium oxide clusters is desired.

Recently, the reactivity of $(ZrO_2)_x^+$ (x=1−4) clusters toward CO, C_2H_4, and C_2H_2 were studied by Johnson and co-workers by means of guided-ion-beam mass spectrometry and density functional theory (DFT) [2]. It was found that $(ZrO_2)_x^+$ clusters have enhanced activity and selectivity for the oxygen transfer reactions, which is attributed to the presence of a radical oxygen center with an elongated zirconium-oxygen bond. Reactions with alkanes (CH_4 and C_2H_6) were also studied, and no oxygen transfer products were observed in the experiments. According to the similarity to the reactions on $V_4O_{10}^+$ and oligomers of $Al_2O_3^+$ [8], they speculated that hydrogen abstraction from alkanes may occur at the radical oxygen centers in $(ZrO_2)_x^+$. However, due to the isotope distribution of zirconium and limitations on mass resolution, hydrogen abstraction cannot be identified in their experiments. What is more, the possibility of hydrogen abstraction from C_2H_4 is not thoroughly considered.

Hydrogen abstraction from alkanes and alkenes yields radical products which are very active and could react to produce many other products. In some cases, it may result in the formation of unwanted byproduct and reduce the catalytic selectivity. To check the possibility of hydrogen abstraction from alkanes and alkenes over transition metal oxide clusters, we have performed a systemic study using the mass spectrometry and the DFT method. Interesting results were obtained. In this work, we focus on the reaction of zirconium oxide clusters with C_2H_4. It demonstrated that hydrogen abstraction may occur for C_2H_4 on $(ZrO_2)_x^+$ (x=1−4).

II. METHODS

A. Experimental methods

The experiments performed in this study were conducted with a time-of-flight mass spectrometer (TOF-

[†]Part of the special issue for "the Chinese Chemical Society's 11th National Chemical Dynamics Symposium".

*Authors to whom correspondence should be addressed. E-mail: shengguihe@iccas.ac.cn, dingxl@iccas.ac.cn,
Tel.: +86-10-62536990, FAX: +86-10-62559373

MS) coupled with a laser ablation/supersonic expansion cluster source and a fast flow reactor [9]. The design of the apparatus was similar to the one used previously [10]. The vacuum system of the apparatus consisted of two chambers. One of the chambers was used for cluster generation/reaction and the other was for cluster ion detection. The two chambers were connected through a 3 mm diameter skimmer. The $Zr_xO_y^+$ clusters were generated by the reaction of laser ablation generated zirconium plasmas with O_2 seeded in the helium (99.999% purity) carrier gas. The typical backing pressure of the He gas was 500 kPa. To generate the metal plasmas, a Nd:YAG laser beam (532 nm, 5 mJ/pulse, 8 ns duration, 10 Hz) was focused onto a zirconium metal disk (16 mm diameter, 3 mm thickness, 99.9% purity, Jiangxi Haite Advanced Material Co., Ltd. China). The disk was rotated and translated to expose a fresh surface continually. The carrier gas seeded with different concentrations of O_2 was controlled by a pulsed valve (General Valve, Series 9). The prepared O_2/He gas mixture passed through a 10 m long copper tube coil with liquid nitrogen temperature before being pulsed into the vacuum chamber. This method almost eliminated the hydrogen impurity peaks ($Zr_xO_yH_z^+$, z>0) that often occured in the cluster distribution. The clusters were formed in a narrow cluster formation channel (2 mm inner diameter) that contained a waiting room (3 mm inner diameter). The lengths of the channel and the waiting room were adjustable to optimize the cluster gr owth conditions. The typical lengths used were 10 mm for the waiting room and 20 mm for the rest of the channel.

A fast flow reactor with 6 mm inner diameter and 61 mm length was coupled with the narrow cluster formation channel. The generated $Zr_xO_y^+$ clusters could exit the empty tube reactor and pass through the 3 mm skimmer for detection through the TOF-MS. Before the detection, the clusters could also react in the tube reactor with reactants (C_xH_y, CO, N_2, *etc.*) diluted in helium carrier gas that was controlled by a second pulsed valve. The cluster ions were extracted, accelerated, and focused by a set of ion optics. The synchronization of laser firing, pulsed valve opening, and ion detection were managed through commercial available and home made electronics. The mass signal was generated by a dual micro-channel plate detector and recorded with a digital oscilloscope (LeCroy WaveSurfer 62Xs). Mass resolution ($M/\Delta M$) of 400−500 was obtained. In this study, we focus on the reaction of $Zr_xO_y^+$ clusters with C_2H_4.

B. Computational methods

The DFT calculations with B3LYP functional [11] were carried out using the Gaussian 03 program [12]. TZVP basis sets [13] were selected for C, H, O atoms, and D95V basis set combined with Stuttgart/Dresden relativistic effective core potential (28-electron core, denoted as SDD in Gaussian 03) was selected for Zr [14].

The DFT calculations were performed for the reactions of $Zr_2O_4^+$ with C_2H_4. Geometry optimization with full relaxation of all atoms was performed. Transition state optimization was performed by using the Berny algorithm [15] from an initial structure obtained through a potential energy surface scan with an appropriate internal coordinate. Vibrational frequency calculations were performed to check that reaction intermediates and transition state species have zero and only one imaginary frequency, respectively. Intrinsic reaction coordinate calculations [16] were also performed to confirm that each transition state connected two appropriate local minima in the reaction paths. The zero-point vibration corrected energies (ΔH_{0K}) and the Gibbs free energies at 298 K (ΔG_{298K}) were reported in this work. Cartesian coordinates, electronic energies, and vibrational frequencies for all of the optimized structures are available upon request.

III. RESULTS

A. Experimental results

The typical mass spectra for reactions of $Zr_xO_y^+$ clusters with 2% C_2H_4 are plotted in Fig1. The generated $Zr_xO_y^+$ clusters can be classified into three series: $Zr_xO_{2x-1}^+$, $Zr_xO_{2x}^+$, and $Zr_xO_{2x+1}^+$, in which x=1−10. Note that due to insufficient mass resolution to resolve Zr isotopomers above 500 a.u., results of large clusters (x>4) are not presented in this work. The most intense product clusters shown in Fig.1 are $Zr_xO_{2x+1}(C_2H_4)^+$ and $Zr_xO_{2x+1}(C_2H_4)_2^+$ that can be

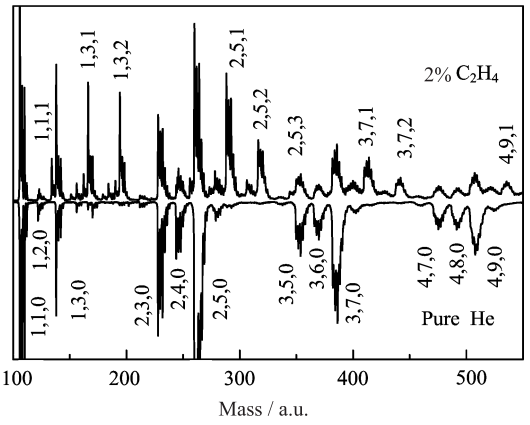

FIG. 1 TOF mass spectra for reaction of $Zr_xO_y^+$ with C_2H_4 in the fast flow reactor. The mass spectra with 2%C_2H_4 and without C_2H_4 being seeded in the helium carrier gas are given in the up and down panels, respectively. 1%O_2 in 500 kPa helium is used to generate the clusters. Symbols x, y, z denote the mass spetrometer detected species $Zr_xO_y(C_2H_4)_z^+$.

DOI:10.1088/1674-0068/22/06/635-641

interpreted respectively as primary and secondary association products of $Zr_xO_{2x+1}{}^+$ reactions with C_2H_4 molecules in the fast flow reactor.

The mass spectra in the Zr_2 region is expanded and re-plotted in Fig.2. The TOF-MS can well resolve the Zr_2 isotopomers (stable isotopes of zirconium: 51.5%^{90}Zr, 11.2%^{91}Zr, 17.1%^{92}Zr, 17.4%^{94}Zr, and 2.8%^{96}Zr). The observed isotopic patterns of $Zr_2O_{3-5}{}^+$ clusters before the reaction match the simulated (pure) Zr_2 isotopomers reasonably well. After the reaction with C_2H_4, the patterns of $Zr_2O_3{}^+$ and $Zr_2O_5{}^+$ do not change within the experimental uncertainties. In sharp contrast, the pattern in the $Zr_2O_4{}^+$ region changes significantly. The intensity of the second peak with mass of $^{90}Zr^{91}ZrO_4{}^+$ is weaker than that of the first one ($^{90}Zr_2O_4{}^+$) before the reaction while it is the opposite after the reaction. As a result, the mass peaks around the $Zr_2O_4{}^+$ region

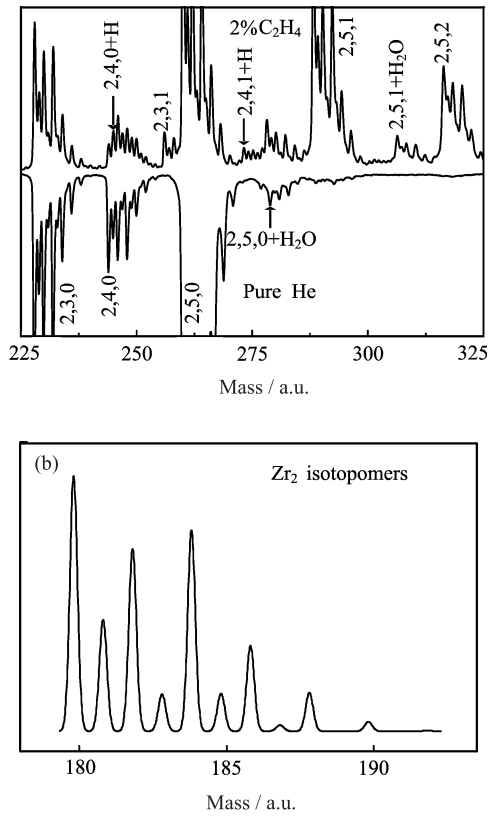

FIG. 2 (a) Re-plot of mass spectra of reaction $Zr_xO_y{}^+$ with C_2H_4 in the $Zr_2O_y{}^+$ region. (b) The simulated Zr_2 isotopomers, the pattern of which is almost the same as those of Zr_2O_3, Zr_2O_4, and Zr_2O_5 since ^{17}O and ^{18}O natural abundance is very low. The first two peaks in the bottom panel of the $Zr_2O_4{}^+$ region are marked and indicated as $^{90}Zr_2O_4{}^+$ and $^{90}Zr^{91}ZrO_4{}^+$. The second peak in the top panel of the $Zr_2O_4{}^+$ region is not purely $^{90}Zr^{91}ZrO_4{}^+$ and it indicates that there is $^{90}Zr_2O_4H^+$ (marked as $^{90}Zr_2O_4{}^+$+H) contribution. Symbols x, y, z denote the mass spetrometer detected species $Zr_xO_y(C_2H_4)_z{}^+$.

after the reaction are not purely due to the $Zr_2O_4{}^+$ isotopomers. Similar results can be found in the regions around $Zr_xO_{2x}{}^+$(x=1, 3, 4), in which the isotopic patterns of the stoichiometric $Zr_xO_{2x}{}^+$(x=1, 3, 4) change significantly upon reaction with C_2H_4 while the non-stoichiometric species $Zr_xO_{2x\pm1}{}^+$ do not change within the experimental uncertainties. The experiment suggests that hydrogen containing clusters, such as $Zr_2O_4H^+$ may be produced in the reaction of $Zr_2O_4{}^+$ with C_2H_4: $Zr_2O_4{}^+ + C_2H_4 \rightarrow Zr_2O_4H^+ + C_2H_3$. Note that Johnson and co-workers identified oxygen transfer channel, such as $Zr_2O_4{}^+ + C_2H_4 \rightarrow Zr_2O_3{}^+ + C_2H_4O$ [2]. Because the peaks of $Zr_2O_3{}^+$ are much more intense than those of $Zr_2O_4{}^+$ in our cluster distribution in Fig.1 and Fig.2, we could not clearly see the signal increase of $Zr_2O_3{}^+$ after the reaction with C_2H_4, due to the scattering of $Zr_2O_3{}^+$ by C_2H_4 and some association of $Zr_2O_3{}^+$ with C_2H_4 in Fig.2. Since the oxygen transfer channel has been reported in detail elsewhere [2], we will not further discuss this channel.

B. Computational results

The result of benchmark calculations with the adopted the DFT method and basis sets is given in Table I. The bond energies of ZrO, ZrO^+, and related main group species can be reasonably reproduced. Then the DFT calculations are performed for the reaction of $Zr_2O_4{}^+$ with C_2H_4. The following two reaction channels are calculated:

$$Zr_2O_4{}^+ + C_2H_4 \rightarrow Zr_2O_4H^+ + CH_2CH\cdot \quad (1)$$
$$\Delta H_{0K} = -0.8 \text{ eV},\ \Delta G_{298K} = -0.82 \text{ eV}$$
$$Zr_2O_4{}^+ + C_2H_4 \rightarrow Zr_2O_3{}^+ + CH_3CHO \quad (2)$$
$$\Delta H_{0K} = -0.73 \text{ eV},\ \Delta G_{298K} = -0.78 \text{ eV}$$

The first one involves a hydrogen abstraction from C_2H_4 to $Zr_2O_4{}^+$, and the second one involves an oxygen transfer from $Zr_2O_4{}^+$ to C_2H_4. The calculated values of enthalpy of formation and change of Gibbs free energy indicate that both of the two channels are thermodynamically allowed. The energies release of the hydrogen

TABLE I Benchmark calculation calculational and experimental data of some critical bond dissociation energies.

Dissociation path	ΔH/eV	
	Calc.	Expt.
^{1}ZrO→^{3}Zr+^{3}O	7.32	7.94 [17]
^{3}ZrO→^{3}Zr+^{3}O	7.46	
^{2}ZrO$^+$→^{2}Zr$^+$+^{3}O	7.33	7.76 [17]
^{2}OH→^{3}O+^{2}H	4.40	4.43 [18]
^{1}C$_2$H$_4$→^{2}C$_2$H$_3$+^{2}H	4.69	4.82 [18]
^{1}CO→^{3}C+^{3}O	10.84	11.16 [17]

*The superscripts indicate the spin multiplicity of the species by italic.

DOI:10.1088/1674-0068/22/06/635-641

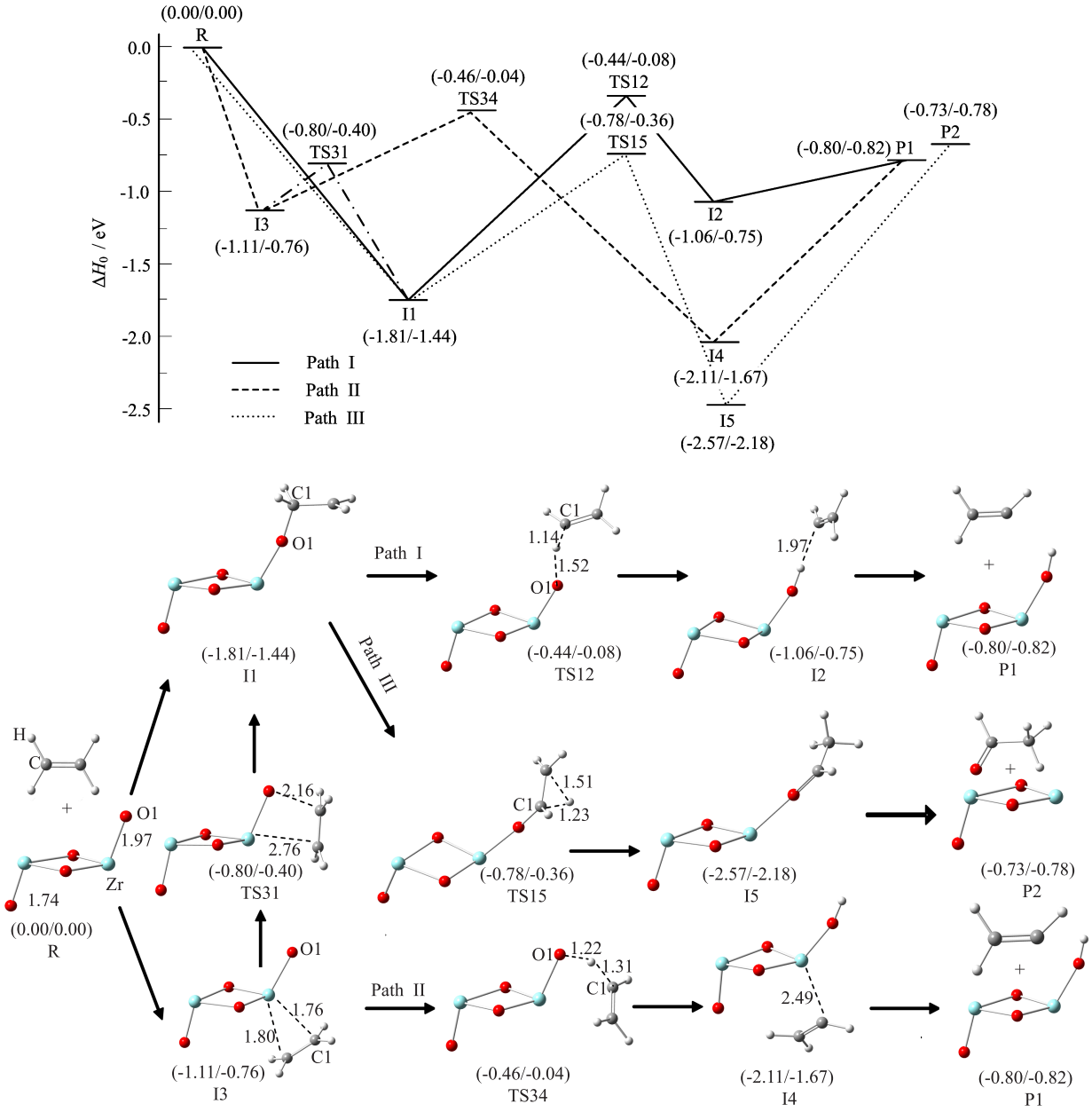

FIG. 3 Calculated potential energy profile of ΔH_{0K} for reactions of $Zr_2O_4^+$ with C_2H_4. The reaction intermediates and transition states are denoted as Ii and TSij, respectively. Energies for each species are given in the brackets as the form ($\Delta H_{0K}/\Delta G_{298K}$). Distances denoted by dashed line are given in Å.

abstraction channel (reaction (1)) is even a little larger than that of the oxygen transfer channel (reaction (2)). So both of the two channels need to be considered in the reaction of $Zr_2O_4^+$ with C_2H_4.

The potential energy profiles of ΔH_{0K} for reaction (1) and reaction (2) are plotted in Fig.3. The structures of the reactants (R), reaction intermediates (Ii), transition states (TSij, between intermediates Ii and Ij), and the two products (P1 and P2) are also given. For each species both ΔH_{0K} and ΔG_{298K} relative to the separated reactants are listed in the brackets.

Three paths are found, in which Path I and II are corresponding to the hydrogen abstraction channel (reaction (1)), and Path III is corresponding to the oxygen transfer channel (reaction (2)). All the three paths are found to be overall barrierless processes, which means that the initial energy of the reactants is sufficient to overcome all the barriers.

Path I in Fig.3 represents the hydrogen abstraction channel with Zr atom being not involved directly. At first, C_2H_4 is adsorbed to the O1 atom as in I1, and a bond is formed between C1 and O1 which is a radical O·. Then a hydrogen atom is transferred from C1 to the O1 atom (TS12), and a CH_2CH· radical is formed

DOI:10.1088/1674-0068/22/06/635-641

TABLE II Rate constants of critical steps at different temperatures (T) obtained from RRKM calculations. The absolute rate constants for reaction I1→I5 (K_{15}) and relative rate constants k_{ij} (k_{ij}=K_{ij}/K_{15}) for reaction Ii→Ij are given. The relative amount of P1 to P2 are listed as [P1]/[P2].

T/K	K_{15}/s^{-1}	k_{12}	k_{34}	k_{31}	k_{13}	[P1]/[P2]
300	1.49×10^{7}	0.051	3.647	490.988	1.323	0.060
400	2.38×10^{7}	0.074	4.018	371.156	1.304	0.088
500	3.96×10^{7}	0.109	4.372	273.464	1.283	0.130
600	6.63×10^{7}	0.159	4.661	199.997	1.262	0.188
700	1.09×10^{8}	0.224	4.872	146.981	1.242	0.264
800	1.76×10^{8}	0.307	5.005	109.299	1.222	0.361

and weakly bound to the transferred H atom. Release of the $CH_2CH\cdot$ needs energy of 0.26 eV.

Path II in Fig.3 represents the hydrogen abstraction channel with Zr atom being involved. At first, C_2H_4 is adsorbed to Zr atom by two C atoms, as in I3. Then a hydrogen atom is transferred from C1 atom to the O1 atom (TS34), and a $CH_2CH\cdot$ radical is formed and firmly bound to the Zr atom. Release of the $CH_2CH\cdot$ needs energy of 1.31 eV.

Path III in Fig.3 represents the oxygen transfer channel. After the adsorption step, which is the same as in Path I, a hydrogen atom is transferred from C1 to the other C atom (TS15), and an acetaldehyde moiety is formed and firmly bound to the Zr atom as in I5. Release of the acetaldehyde needs energy of 1.84 eV. Path III was also considered by Johnson and co-workers [2]. Their relative energies are 0.00, −1.90, −0.79, −2.67, and −0.80 eV for R, I1, TS15, I5, and P2, respectively. Our results with/without zero-point energy corrections for these species are 0.00, −1.81/−1.88, −0.78/−0.77, −2.57/−2.67, and −0.73/−0.79 eV respectively, which are very close (within 0.1 eV) to theirs.

I1 and I3 are two possible adsorption structures of C_2H_4 on $Zr_2O_4^+$. They can be converted to each other through a transition state (TS31). This conversion is very important and will be discussed more in the following section.

IV. DISCUSSION

The calculations indicate that hydrogen abstraction channel (reaction (1)) and oxygen transfer channel (reaction (2)) are two competing channels of $Zr_2O_4^+$+C_2H_4. The Rice-Ramsberger-Kassel-Marcus (RRKM) theory [19] can be used for estimation of rate constants of the two reaction channels. The rate constants of five critical steps, *i.e.*, I1→I2, I1→I5, I3→I4, I3→I1, and I1→I3 (denoted as K_{ij} for reaction Ii→Ij) are computed with RRKM theory. In these calculations, the energy of the initially formed reaction intermediates (E) and the energy barrier ($E^{\neq}$) for each step are needed. The initially formed meta-stable reaction intermediates I1 and I3 carry not only the binding energy (E_b) between $Zr_2O_4^+$ and C_2H_4, but also the vibrational energies (E_{vib}) of $Zr_2O_4^+$ and C_2H_4 at particular temperature (T), and the center of mass kinetic energy (E_k). That is,

$$E = E_b + E_{vib}(Zr_2O_4^+) + E_{vib}(C_2H_4) + E_k \quad (3)$$

Then the rate constant is calculated as:

$$k(E) = \frac{gN^{\neq}(E-E^{\neq})/\rho(E)}{h} \quad (4)$$

in which g is the symmetry factor (g=2 for the first of three steps and g=1 for the later two steps), $\rho(E)$ denotes the density of states of the meta-stable intermediates at the energy E, $N^{\neq}(E-E^{\neq})$ is the total number of states of the transition state (activated complex), and h is the Planck constant. The direct count method proposed by Beyer and Swinehart [20] was used for determining the number ($N^{\neq}$) and density (ρ) of states under the approximation of harmonic vibrations. The values of E_{vib}, E_b, $E^{\neq}$, and vibrational frequencies are all obtained from DFT calculations, and E_k=$\mu v^2/2$, in which μ is the reduced mass of $Zr_2O_4^+$ and C_2H_4 and the velocity v estimated as 1 km/s. Both E_b and $E^{\neq}$ are zero-point-vibration corrected energies.

The calculated rate constants of these critical steps at different temperatures obtained from RRKM calculations are listed in Table II. The absolute rate constant for reaction I1→I5 (K_{15}) and relative rate constants k_{ij} (k_{ij}=K_{ij}/K_{15}) are given for the other reactions. The values of K_{12} are smaller than those of K_{15}, but the ratio (k_{12}) increases with the increasing of T, which indicates that hydrogen abstraction from C_2H_4 through Path I prefers high T. The values of K_{34} are larger than those of K_{15}, but due to a much quicker channel from I3 to I1 (large k_{31}), there is only a little chance for the reaction I3→I4 to happen.

For the direct dissociation steps (from I2, I4, or I5 to P1 or P2), there are no distinct transition states on the potential energy surface. The rate constants of these steps are estimated by the variational transition state theory [19], and are found to be at least 3 orders of magnitude larger than K_{15}. So the rate-limiting steps are the H-transfer or O-transfer steps.

After the initial meta-stable species $Zr_2O_4C_2H_4^+$/I1 or $Zr_2O_4C_2H_4^+$/I3 are formed, the population possibilities [I1] and [I3] of I1 and I3 with respect to time can

DOI:10.1088/1674-0068/22/06/635-641

be modeled with the following coupled equations:

$$\frac{\mathrm{d[I1]}}{\mathrm{d}t} = -K_{12}[\mathrm{I1}] - K_{15}[\mathrm{I1}] - K_{13}[\mathrm{I1}] + K_{31}[\mathrm{I3}] \quad (5)$$

$$\frac{\mathrm{d[I3]}}{\mathrm{d}t} = -K_{34}[\mathrm{I3}] - K_{31}[\mathrm{I3}] + K_{13}[\mathrm{I1}] \quad (6)$$

The amount of P1 formation in unit time ([P1]) from Path I is K_{12}[I1], and the amount [P2] of P2 is K_{15}[I1]. The ratio K_{12}[I1]/K_{15}[I1] equals to k_{12}, which is listed in Table II. P1 can also be formed from Path II, and the amount is K_{34}[I3]. From the values of total ratio [P1]/[P2] and k_{12} in Table II, we can see that the contribution to the formation of P1 from Path II ([P1]/[P2]$-k_{12}$) is quite small. This is mainly due to the very low energy barrier from I3 to I1, leading to the very low population of I3 with respect to that of I1. The total ratio [P1]/[P2] is relatively small at 300 K, and increases with the increasing of T. At high temperatures (above 500 K, note that vibrational temperature of VO_2 can be as high as 700 K [21]), the hydrogen abstraction from C_2H_4 becomes more and more favorable. Taking also account of the uncertainties of the DFT calculated reaction barriers, our theoretical results support that the hydrogen containing product $Zr_2O_4H^+$ shown in Fig.2 can be from the hydrogen abstraction from ethylene (reaction (1)).

For alkenes, the C=C π bond is expected to be much more reactive than the C−H σ bond and the activation of the C=C bond by reactive oxygen atom tends to cause oxygen transfer reaction such as Path III in Fig.3. As a result, the hydrogen abstraction from alkenes is usually not expected. There are not many reported examples of hydrogen abstraction from alkenes in the cluster reactivity studies. Heinemann *et al.* observed hydrogen abstraction from propylene (C_3H_6) and butenes (C_4H_8) by CeO_2^+ [22]. Due to very high activity of the stoichiometric zirconium oxide cations ($Zr_xO_{2x}^+$) [2], our experimental and theoretical studies in Fig.2 and Fig.3 suggest that hydrogen abstraction from C_2H_4 by $Zr_2O_4^+$ is possible.

V. CONCLUSION

The study of reactions of $Zr_xO_y^+$ with C_2H_4 in the fast flow reactor has identified the appearance of hydrogen containing clusters $(ZrO_2)_xH^+(x=1-4)$ from the reactions. The DFT calculations support that $(ZrO_2)_xH^+$ may be produced from $(ZrO_2)_x^+$+C_2H_4 by a hydrogen abstraction process. Reaction rate calculations by RRKM theory indicate that the hydrogen abstraction channel prefers at high temperatures. This work reveals a new possible reaction channel of alkenes on $(ZrO_2)_x^+$ clusters, which may be extended to other transition metal oxide clusters.

VI. ACKNOWLEDGEMENTS

This work was supported by the Hundred Talents fund of The Chinese Academy of Sciences, the National Natural Science Foundation of China (No.20703048, No.20803083, and No.20933008), the Center for Molecular Science Foundation of Institute of Chemistry, Chinese Academy of Sciences (No.CMS-CX200803), and the National Basic Research Programs of China (No.2006CB932100 and No.2006CB806200).

[1] (a) W. Xue, Z. C. Wang, S. G. He, Y. Xie, and E. R. Bernstein, J. Am. Chem. Soc. **130**, 15879 (2008).
(b) F. Dong, S. Heinbuch, Y. Xie, J. J. Rocca, E. R. Bernstein, Z. C. Wang, K. Deng, and S. G. He, J. Am. Chem. Soc. **130**, 1932 (2008).
(c) F. Dong, S. Heinbuch, Y. Xie, E. R. Bernstein, J. J. Rocca, Z. C. Wang, X. L. Ding, and S. G. He, J. Am. Chem. Soc. **131**, 1057 (2009).
[2] G. E. Johnson, R. Mitric, E. C. Tyo, V. Bonacic-Koutecky, and A. W. Castleman, Jr., J. Am. Chem. Soc. **130**, 13912 (2008).
[3] S. N. Khanna and P. Jena, Phys. Rev. Lett. **69**, 1664 (1992).
(b) S. N. Khanna and P. Jena, Phys. Rev. B **51**, 13705 (1995).
(c) A. W. Castleman, Jr. and P. Jena, Proc. Natl. Acad. Sci. USA **103**, 10552 (2006).
(d) A. W. Castleman, Jr. and P. Jena, Proc. Natl. Acad. Sci. USA **103**, 10554 (2006).
[4] (a) J. Zhu, J. G. van Ommen, and L. Lefferts, Catal. Today **112**, 82 (2006).
(b) J. J. Zhu, J. G. van Ommen, H. J. M. Boumeester, and L. Lefferts, J. Catal. **233**, 434 (2005).
[5] M. M. Yung, E. M. Holmgreen, and U. S. Ozkan, Catal. Lett. **118**, 180 (2007).
[6] G. Jin, G. Lu, Y. Guo, J. Wang, and X. Liu, Catal. Today **93**, 173 (2004).
[7] (a) K. A. Zemski, D. R. Justes, and A. W. Castleman, Jr., J. Phys. Chem. B **106**, 6136 (2002).
(b) D. K. Bohme and H. Schwarz, Angew. Chem. Int. Ed. **44**, 2336 (2005).
[8] (a) S. Feyel, D. Schroder, and H. Schwarz, J. Phys. Chem. A **110**, 2647 (2006).
(b) S. Feyel, J. Dobler, R. Hokendorf, M. K. Beyer, J. Sauer, and H. Schwarz, Angew. Chem. Int. Ed. **47**, 1946 (2008).
[9] M. E. Geusic, M. D. Morse, S. C. O'Brien, and R. E. Smalley, Rev. Sci. Instrum. **56**, 2123 (1985).
[10] (a) W. G. Wang, Z. C. Wang, S. Yin, S. G. He, and M. F. Ge, Chin. J. Chem. Phys. **20**, 412 (2007).
(b) S. Yin, Y. P. Ma, L. Du, S. G. He, and M. F. Ge, Chin. Sci. Bull. **53**, 3829 (2008).
(c) S. Yin, W. Xue, X. L. Ding, W. G. Wang, S. G. He, and M. F. Ge, Int. J. Mass Spectrom. **281**, 72 (2009).
(d) W. Xue, S. Yin, X. L. Ding, S. G. He, and M. F. Ge, J. Phys. Chem. A **281**, 72 (2009).
[11] A. D. Becke, J. Chem. Phys. **98**, 5648 (1993).

DOI:10.1088/1674-0068/22/06/635-641

[12] M. J. Frisch, G. W. Trucks, H. B. Schlegel, G. E. Scuseria, M. A. Robb, J. R. Cheeseman, G. Scalmani, V. Barone, B. Mennucci, G. A. Petersson, H. Nakatsuji, M. Caricato, X. Li, H. P. Hratchian, A. F. Izmaylov, J. Bloino, G. Zheng, J. L. Sonnenberg, M. Hada, M. Ehara, K. Toyota, R. Fukuda, J. Hasegawa, M. Ishida, T. Nakajima, Y. Honda, O. Kitao, H. Nakai, T. Vreven, J. A. Montgomery Jr., J. E. Peralta, F. Ogliaro, M. Bearpark, J. J. Heyd, E. Brothers, K. N. Kudin, V. N. Staroverov, R. Kobayashi, J. Normand, K. Raghavachari, A. Rendell, J. C. Burant, S. S. Iyengar, J. Tomasi, M. Cossi, N. Rega, J. M. Millam, M. Klene, J. E. Knox, J. B. Cross, V. Bakken, C. Adamo, J. Jaramillo, R. Gomperts, R. E. Stratmann, O. Yazyev, A. J. Austin, R. Cammi, C. Pomelli, J. W. Ochterski, R. L. Martin, K. Morokuma, V. G. Zakrzewski, G. A. Voth, P. Salvador, J. J. Dannenberg, S. Dapprich, A. D. Daniels, O. Farkas, J. B. Foresman, J. V. Ortiz, J. Cioslowski, and D. J. Fox, *Gaussian 03*, *Revision C.* 02, Pittsburgh, PA: Gaussian, Inc., Wallingford CT. (2004).
[13] A. Schaefer, C. Huber, and R. Ahlrichs, J. Chem. Phys. **100**, 5829 (1994).
[14] D. Andrae, U. Haeussermann, M. Dolg, H. Stoll, and H. Preuss, Theor. Chim. Acta **7**, 123 (1990).
[15] H. B. Schlegel, J. Comput. Chem. **3**, 214 (1982).
[16] (a) C. Gonzalez and H. B. Schlegel, J. Chem. Phys. **90**, 2154 (1989).
(b) C. Gonzalez and H. B. Schlegel, J. Chem. Phys. **94**, 5523 (1990).
[17] H.P. Loock, B. Simard, S. Wallin, and C. Linton, J. Chem. Phys. **109**, 8980 (1998).
[18] D. R. Lide, *CRC Handbook of Chemistry and Physics*, 84th edn., Boca Raton: CRC Press, 799 (2003).
[19] J. I. Steinfeld, J. S. Francisco, and W. L. Hase, *Chemical Kinetics and Dynamics, Upper Saddle River*, New Jersey: Prentice-Hall, 231 (1999).
[20] T. Beyer and D. R. Swinehart, Comm. Assoc. Comput. Machines **16**, 379 (1973).
[21] Y. Matsuda and E. R. Bernstein, J. Phys. Chem. A **109**, 3803 (2005).
[22] C. Heinemann, H. H. Cornehl, D. Schröder, M. Dolg, and H. Schwarz, Inorg. Chem. **35**, 2463 (1996).

DOI:10.1088/1674-0068/22/06/635-641